LA-UR-14-28325
Approved for public release; distribution is unlimited.

Title: Production Facility Beam Line Design Report

Author(s): Bishofberger, Kip A.

Intended for: Report

Issued: 2014-10-24

Electron Accelerator Mo-99 Production Facility Beam Line Design Report

GTRI WBS 21.2.94.1.4 Activity 4 Deliverable 2 (A1618D2)
Kip Bishofberger
version 4: Oct 22, 2014

The following simulations use a single beamline model that matches the beam profile from the exit of the 42-MeV accelerator to the necessary target size. Shown below, this beamline consists of the following elements:

1) The copper-cavity accelerator accelerates the beam to 42 MeV.
2) A quadrupole matching unit enables size adjustment.
3) A non-dispersive set of three bend magnets, which bends the beam 20 degrees total.
4) A quad doublet for final beam focusing to the target.
5) A conversion section based on nonlinear optics, which converts the Gaussian profile into a more flattop shape at the target.

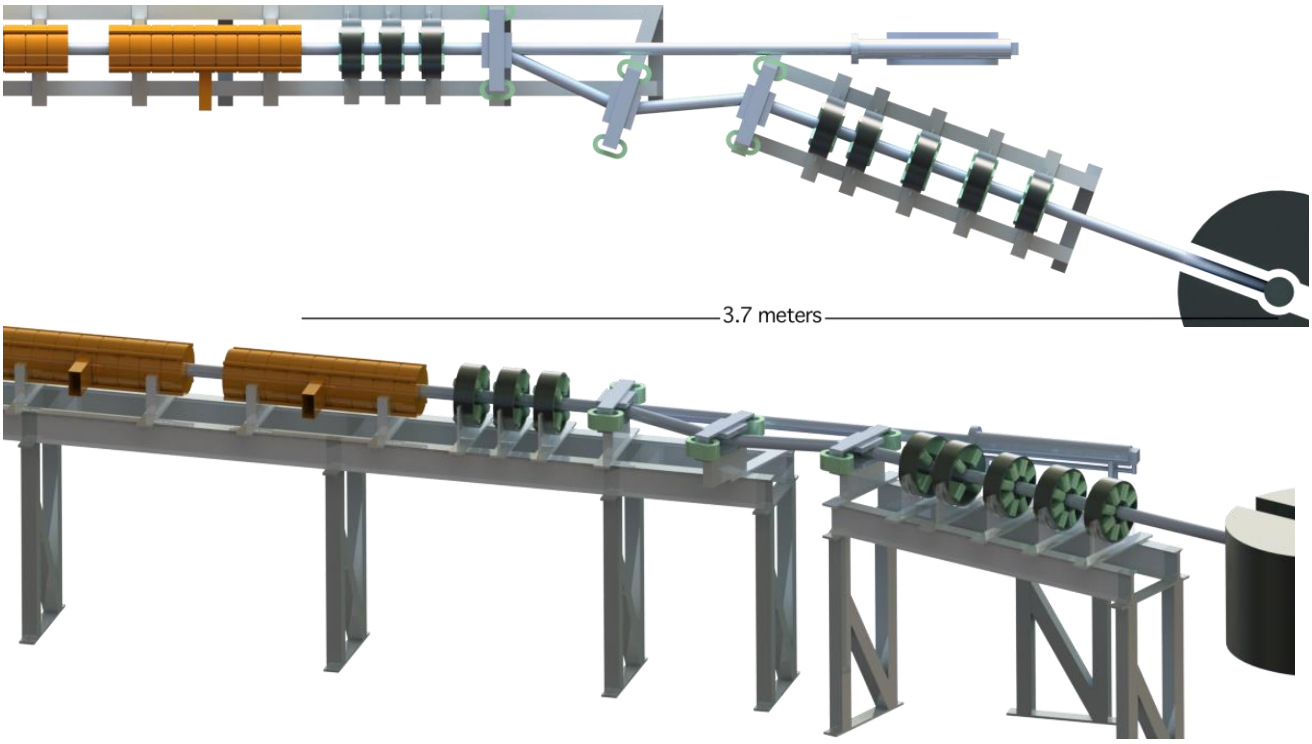

The above models show the design beamline used in the following scenarios; the simulations start at the exit of the copper accelerator. The simulations use Marylie/Impact, which incorporates fifth-order nonlinearities in magnetic elements. The physical geometry of the beamline remains un-changed for all of the simulations. The nominal beam parameters, exiting the accelerator, are as follows:

transverse beta-function	0.7 m
transverse emittance, norm.	6 or 9 μm RMS
avg. kinetic energy	42 MeV
energy spread	3% FWHM
beam size	6 mm FWHM

The following scenarios involved adjusting quadrupole and nonlinear-element strengths. In each case, the overall goal was to match the beam size to a specific size, but reduce the "Gaussian tails" on the edge of the beam.

Scenario 1: 42-MeV, 9-um emittance, 12-mm FWHM

The following figures show the beam behavior for the nominal beam energy, a beam size of 12 mm, and a relatively large emittance of 9-um.

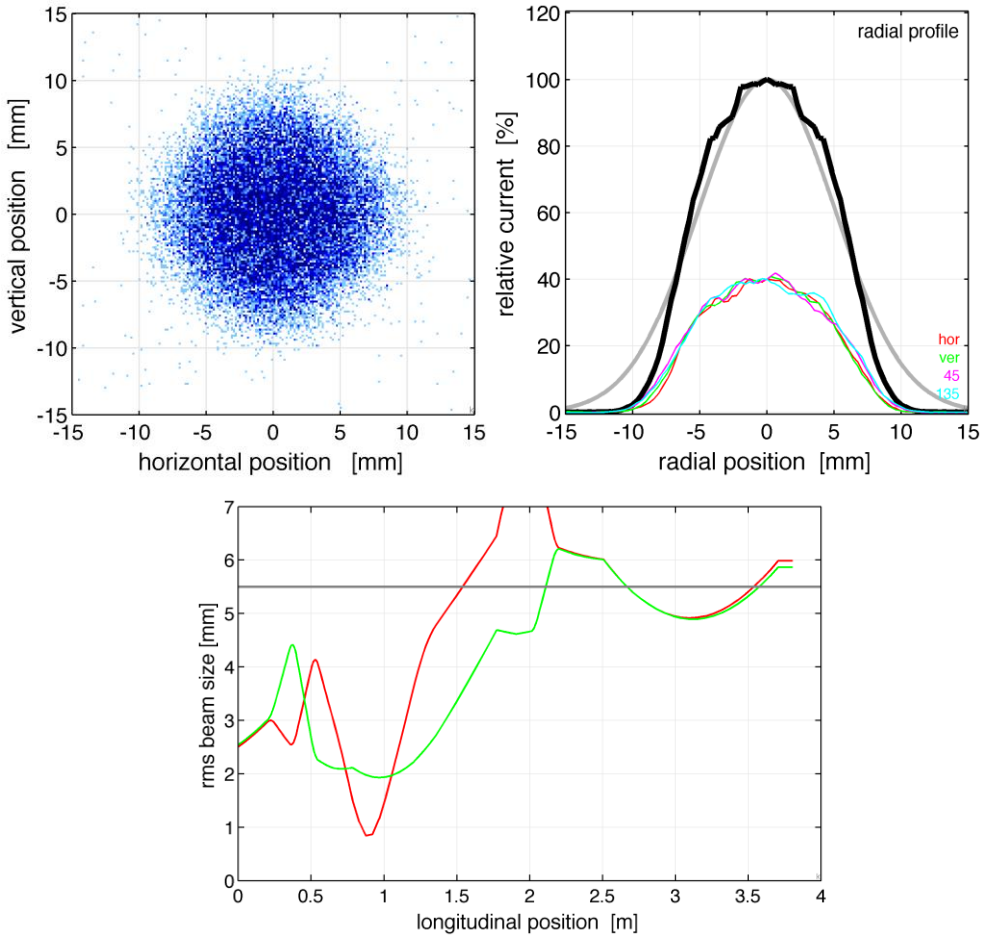

The upper-left figure shows the spot on target. This beam appears circular, relatively uniform without any narrow peak, and reasonably contained.

The second figure studies the same beam profile more quantitatively. The heavy black line is the radial profile calculated from all of the particles. A grey curve is also shown which represents a 12-mm FWHM Gaussian beam. For the same peak intensity at the center, this profile shows a drastic reduction in the current density from the Gaussian tails. Instead, those tails have been folded into the shoulders of the central beam portion, creating a more compact and flattop profile than a typical Gaussian.

On a smaller scale, the second plot also shows profiles along the horizontal (red), vertical (green), 45-degree (magenta), and 135-degree (cyan) sections. The fact that these traces are nearly identical confirms the circular shape of this beam.

The third figure simply tracks the beam size through the entire matching section (RMS). The first set of quadrupoles in in the first 0.5 meters, followed by about a meter in the bending section. The

quadrupole doublet ends at ~2.2 meters, followed by another 0.5 meters for the octopole section. Finally, over a meter of free drift is provided as the beam enters the shielded target section.

The following plots show four beam profiles as the octopole strength is increased.

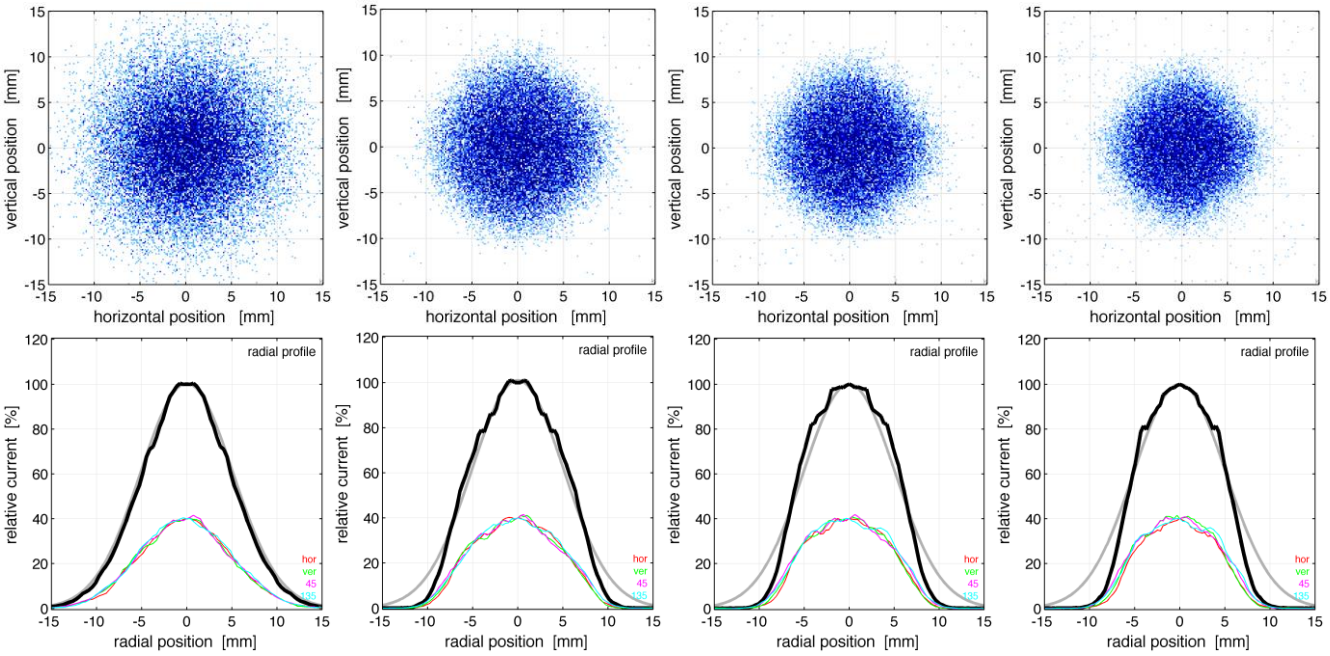

The two plots on the far left shows the profile with the octopoles completely off; the profile matches the Gaussian curve very well, including the tails at large radii. By turning on the octopoles and increasing their strength, the profile's tails are dramatically reduced, and the beam power is more uniformly distributed through the beam core.

Scenario 2: 42-MeV, 6-um emittance, 12-mm FWHM

There are two methods to improve the flatness of the beam profile at the target without significant beam interception: reduction of the emittance and expansion of the beam size. This scenario studies the effect of a 33% improvement in the beam emittance as compared to the previous case. The following profiles are again in order of increasing octopole strength.

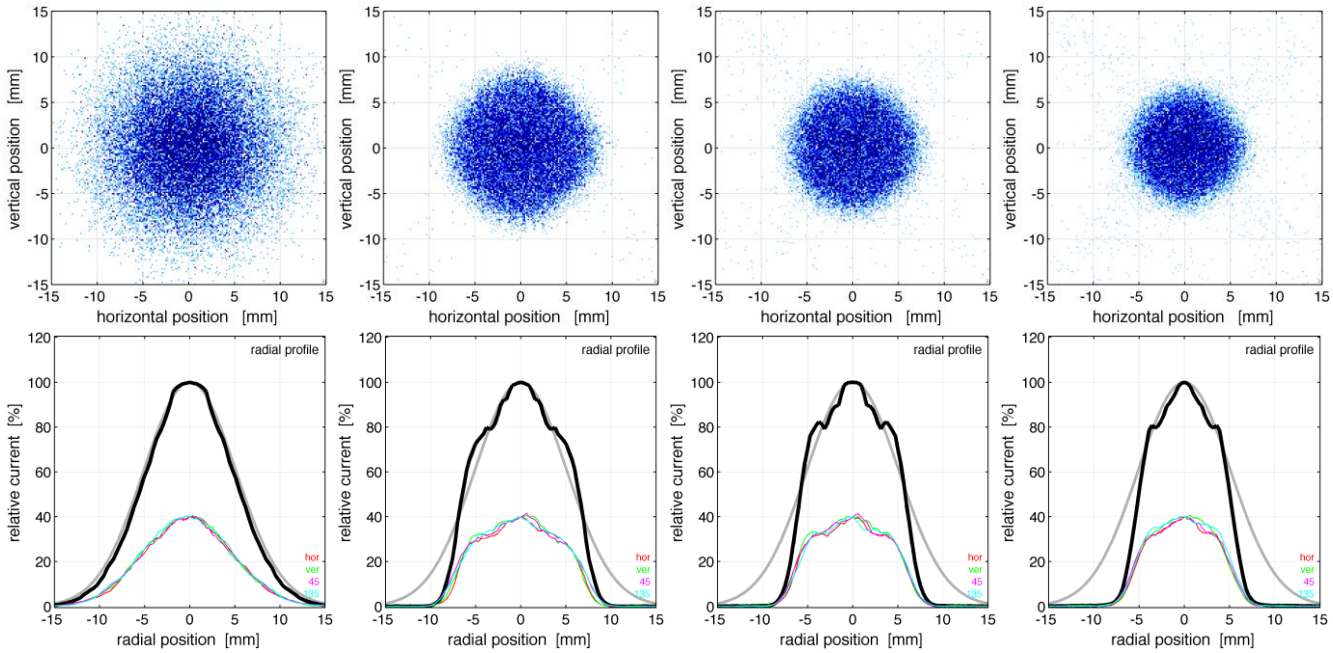

The two plots on the far left illustrate the Gaussian-like profile with the octopoles turned off. Proceeding to the right, the octopole strength increases. The shape of the profile is noticeably more rectangular than the higher-emittance simulations: the central portion is more flat, and the sides are sharper.

Scenario 3: 42-MeV, 9-um emittance, larger target sizes

Increasing the beam radius is the second way to enable a more flattop profile at the target. It has been found that the effectiveness is stronger than changing the emittance. The following figures represent a 24-mm FWHM beam.

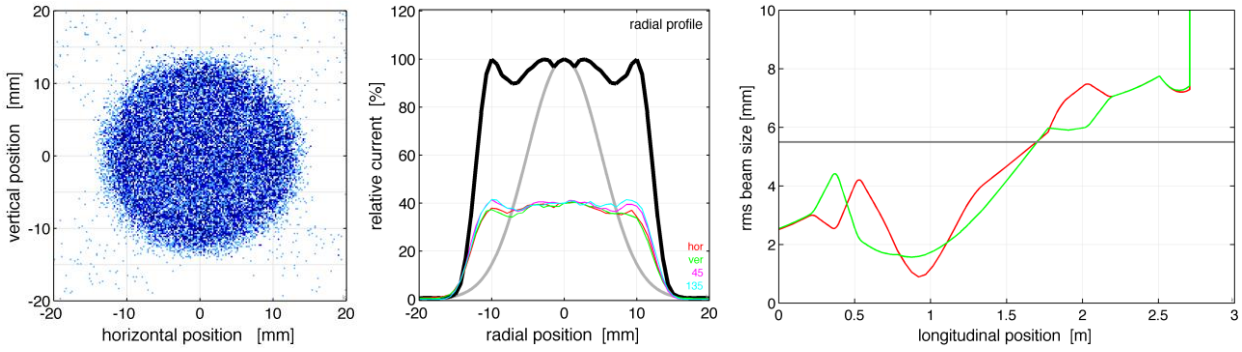

The beam is significantly flatter and more rectangular than other scenarios. Flexing the strength of the octopoles can alter the small "horns" on the edge of the beam.

A beam designed for a 30-mm beam size on target also exhibits a similar profile, as the first two plots below show.

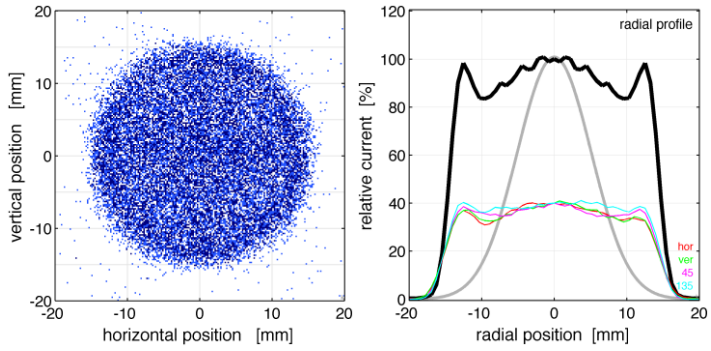

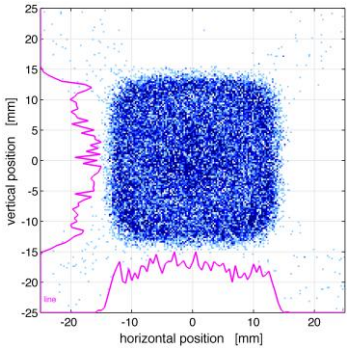

The plot on the right shows a square shaped beam, simply by adjusting the nonlinear settings. It is important to remember that these scenarios utilize the same physical beamline layout as the 12-mm scenarios; only various focusing strengths are being manipulated.

Scenario 4: Varying energy and energy spread

The 20-degree bend section is non-dispersive by design, so that significant changes in beam energy, including higher energy spread, will be steered exactly the same amount. Focusing the different energies is more difficult, so we expect the beam shape to be altered somewhat. The following two situations show the effect of increasing energy spread.

The next two plots show the results of a 3%-FWHM energy spread, which is the basis for all prior scenarios as well. This nominal amount of energy spread does not adversely affect the profile.

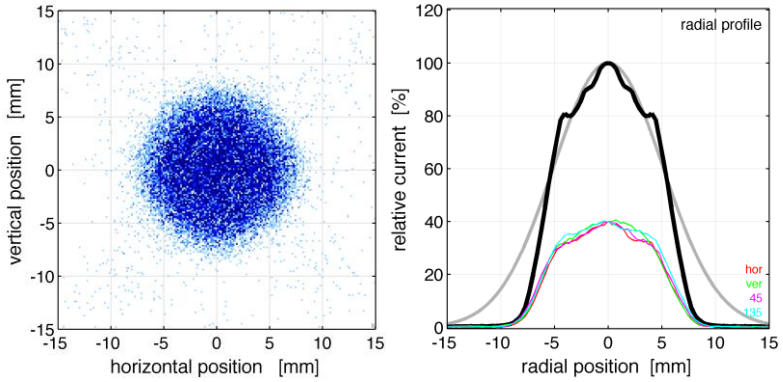

The following three plots show the effect of a 6%-FWHM energy spread. The difference between 3% and 6% is barely noticeable.

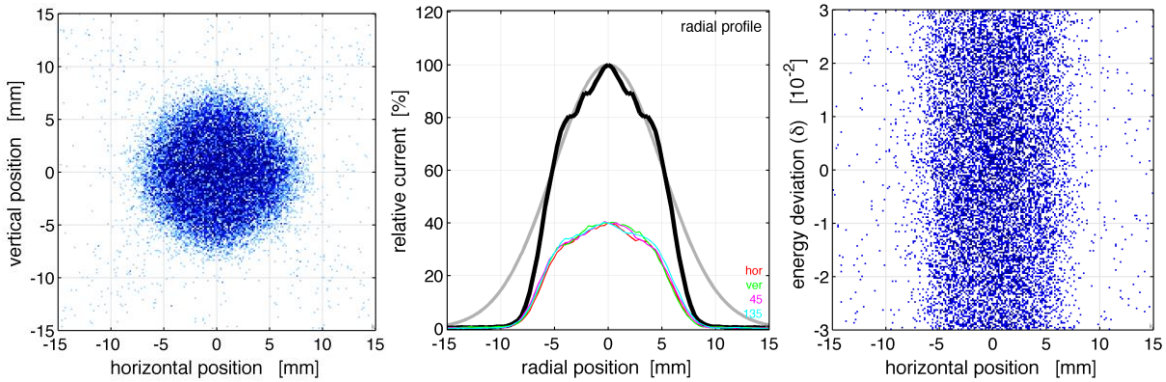

The right plot, which compares particle position with their energy, explains the reason for the stability. Typically, a bend magnet is highly dispersive, so that particles of high energy would be horizontally displaced in one direction, while particles with low energy would be displaced in the other; the blue stripe above would exhibit a large. However, in this optimized beamline design, the bend section provides zero dispersion; particles stay at the same horizontal position regardless of their energy, and the stripe in the plot is perfectly vertical.

Fluctuations in beam energy can also affect the size of the beam. The previous analysis shows very little change in beam size from 3% to 6% energy spread. The following simulations study the beam sizes for different average energies. The middle column shows the nominal 42-MeV beam (with 3%-FWHM spread). The left column is the result of a 41-MeV beam, while the right column is the result of a 43-MeV beam. Over this wide range of energies, the beam size changes less than 4%.

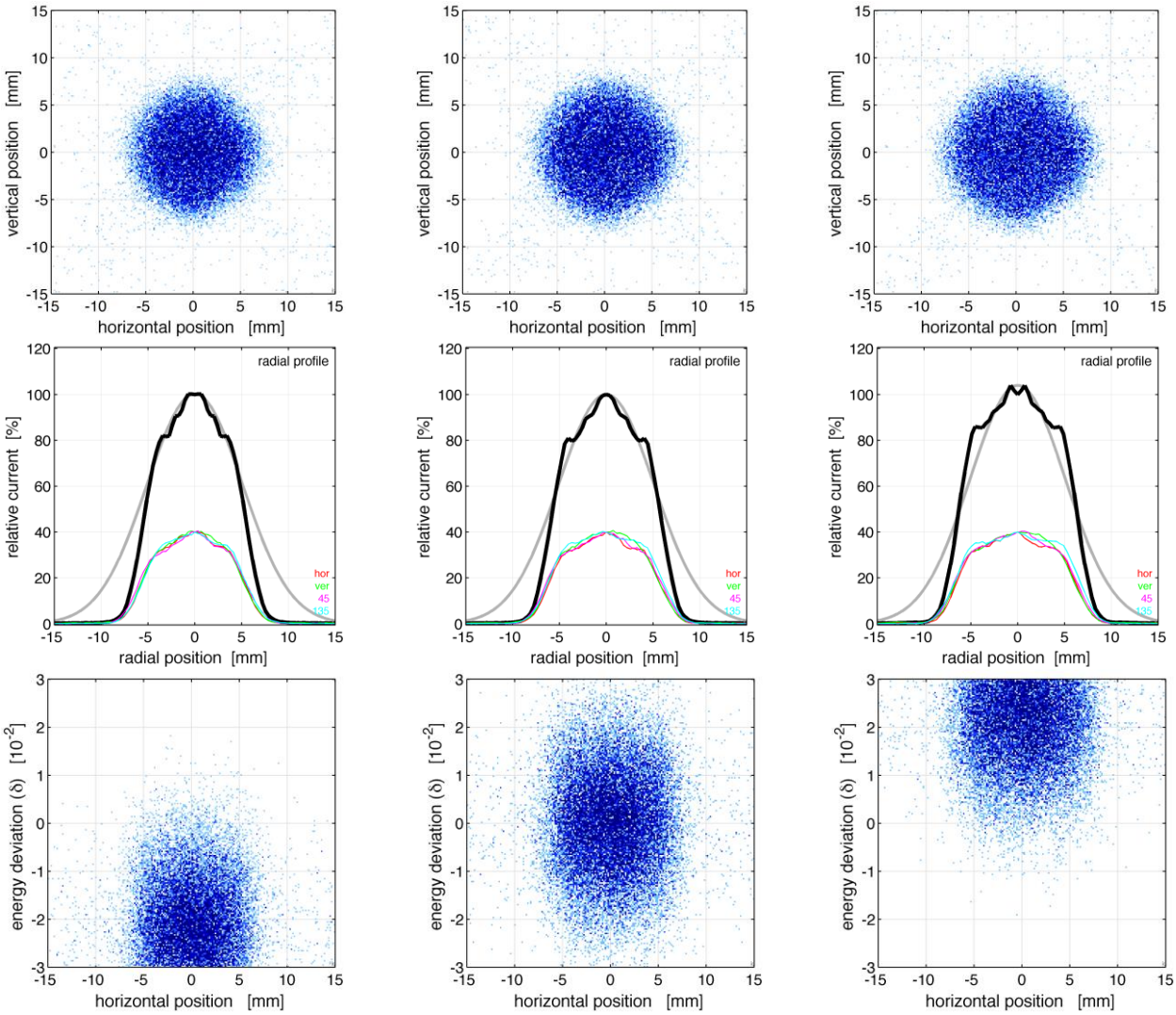

In typical accelerators, small energy fluctuations (~0.2%) are not uncommon, but increasing beam current in the accelerator might lead to a systemic decrease in energy (due to beam loading), affecting beam profile. Optimizing the focusing elements for the full beam current eliminates this concern.

Scenario 5: Beam misalignment

Since all beamlines have nonzero positional jitter, it's important to know the effect on the beam position and size at the target. However, the current design is arranged so that an initial positional error actually has little effect on the position at the target (in beam physics, the Twiss phase is nearly zero). Instead, the beam is steered at an angle; but the amount is far less than a typical target will detect. The following simulations show the effect of an initial horizontal beam offset.

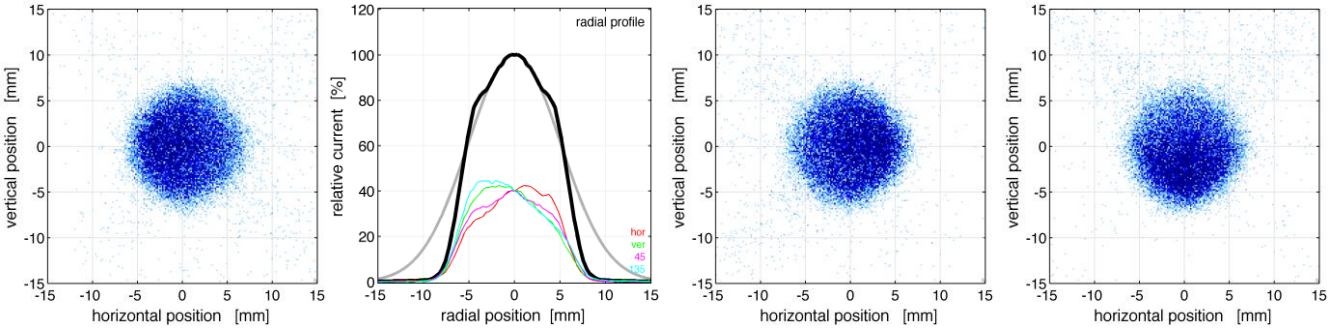

The first two figures show the profile when the initial beam was off center by +1 mm. The particle distribution is slightly asymmetric, while remaining confined in the same 12-mm envelope. The radial profile, which averages distributions across all axes, remains relatively unchanged, but the horizontal (and angled) cross-section profiles are also shown (in different colors) to illustrate this variation. It can be seen that from the left to the right side, there is approximately a 20% variation in current density.

The next figure illustrates the result of an initial offset of –1 mm; it is essentially the +1-mm scenario in reverse. The final figure is the distribution with an initial vertical offset of +1 mm, again mimicking the original profile. In all cases, the total distribution remains within the original target boundary. A systematic offset can be detected using the OTR or IR target diagnostics, or the beam position monitors, and can be easily remedied with beam steering magnets.

More often, beams exit accelerators with correlated transverse and angle offsets. The following simulations study two different correlated offsets due to misalignment.

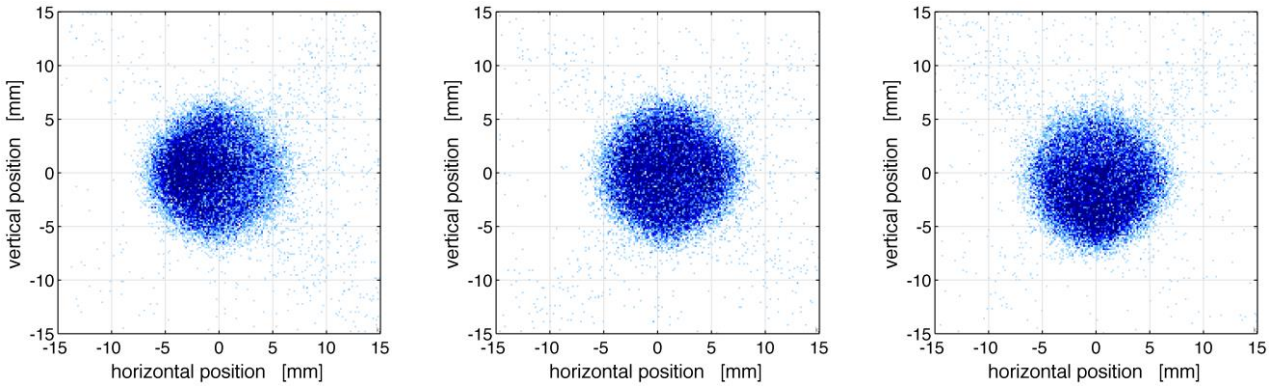

The first figure shows the beam at the target for an initial offset of +1 mm and +1.4 mrad. It can be observed that the beam's asymmetry is slightly increased over just the translation case, but still remaining confined in the centered 12-mm envelope. The second case also initiates with +1 mm offset, but –1.4 mrad, as if there is nonzero focusing inside the accelerator section. In this case, the

asymmetry is nearly eliminated. There is a possibility that either of these scenarios can occur; an accelerator section can be designed to provide a positive or negative correlation (alpha) at its output.

The third plot shows a similar offset of +1 mm and +1 mrad, but this time in the vertical plane.

The fact that these asymmetries are well confined is useful for ensuring the beam centroid remain centered on the target. Shot-to-shot variations will average to a uniform beam without sending excessive beam outside the target area.

Diagnostics Effort

Simultaneously with beamline optimization, several diagnostic tools have been listed for verifying performance of the production beamline. Verifying beam position is perhaps the most important concern. The picture below shows a bpm designed for this beamline. It has been constructed and is now being tested.

At a minimum, one viewing screen and an energy spectrometer is necessary to verify beam profile and energy spread. Collimators and beam loss monitors also provide machine safety. The beamline will also include two current monitors to verify beam transmission. The target itself is monitored by OTR and IR diagnostics that provide sophisticated monitoring of the production in real time. Finally, the initial accelerator section requires RF feedback for stable particle acceleration.

Conclusions

The simulations discussed in this report show that this particular beamline design achieves a unique distribution at the target. Nonlinear optics provides a more flattop beam profile across the target area than a simple Gaussian, yet it does not require significant collimation. The single beamline design is capable of producing a variety of beam sizes and shapes, using only changes in magnet strengths.

Most importantly, the beamline design stabilizes the beam position and size over a large range of energy, position, and direction errors in the actual beam. At a production facility where the beam current is maximized, beam stability at the target is critical for reliable operation. Thermal modeling of this beam shape on the target is ongoing, as is developing engineering designs for specific components and testing of diagnostics systems.